Chinese Journal of Chemical Engineering 56 (2023) 70–79

Contents lists available at ScienceDirect

Chinese Journal of Chemical Engineering

journal homepage: www.elsevier.com/locate/CJChE

Full Length Article

Experimental investigation on degradation mechanism of membrane electrode assembly at different humidity under automotive protocol

Jiajun Wang [1,2], Wenbin Yang [1,2], Jiangtao Geng [1,*], Zhigang Shao [1,*], Wei Song [1]

[1] Fuel Cell System and Engineering Laboratory, Key Laboratory of Fuel Cells and Hybrid Power Sources, Dalian Institute of Chemical Physics, Chinese Academy of Sciences, Dalian 116023, China
[2] University of Chinese Academy of Sciences, Beijing 100039, China

ARTICLE INFO

Article history:
Received 8 April 2022
Received in revised form 15 July 2022
Accepted 19 July 2022
Available online 13 September 2022

Keywords:
Fuel cell
Simulating automotive protocol
Relative humidity
Degradation
Membrane

ABSTRACT

Humidity can affect the attenuation of MEA (membrane electrode assembly), however, the relationship between humidity and MEA decays is complex and ambiguous in realistic application. Herein, we design a simulating automotive protocol, performed on five single fuel cells under RH (relative humidity) 100%, RH 80%, RH 64%, and RH 40%, RH 10%, respectively, to study the relationship of MEA decays and humidity and suggest optimized humidity range to extend the durability. With the electrochemical impedance spectroscopy, cyclic voltammetry, X-ray fluorescence, X-ray diffraction, transmission electron microscope, X-ray photoelectron spectroscopy, the four degradation mechanisms about catalyst layer, including Pt dissolution, Pt coarsening, carbon corrosion and ionomer degradation, are observed. Pt coarsening and carbon corrosion are accelerated by higher water content at high humidity. Ionomer degradation and Pt dissolution are enhanced in low humidity. With the linear sweep voltammetry, ion chromatography, nuclear magnetic resonance, tensile test and scan electron microscope, chemical and mechanical degradation in proton exchange membrane are all observed in these five fuels. Chemical degradation, characterized by membrane thinning and more fluoride loss, occurred markedly in RH 10%. Mechanical degradation, characterized by the non-uniformity thickness and bad mechanical properties, is more pronounced in RH 100%, RH 80%, RH 64%. These two degradations are in a moderate level in RH 40%. The research suggests that the RH range from 64% to 40% is conductive to mitigate the degradation of MEAs operated in automotive applications.

1. Introduction

PEMFC (Proton exchange membrane fuel cell) is an environmentally friendly energy conversion device with high energy transform efficiency and low operating temperature [1]. However, high cost and insufficient durability hinder seriously the commercialization of PEMFC [2]. Since the degradation of MEAs affects directly the durability during long term operation, the key of improving lifetime is MEAs, including PEM (proton exchange membrane), CL (catalyst layer) and GDL (gas diffusion layer). More generally, GDL degradation will lead to voltage drop at high current density [3]. The degradation rate of GDL is about 10^{-10} [4], therefore, the CL and PEM attenuation be more discussed. Under automotive condition, PEMFC runs in dynamic load, inducing (1) humidity and thermal cycling, (2) gas starvation, and (3) potential cycling, causing chemical and mechanical degradation not only to PEM, but to CL.

PEM degradation, including mechanical, chemical, and thermal modes, will lead to H_2 crossover and eventually the failure of PEMFC [5–7]. The attenuation of PEM is affected by many factors and humidity is the most influential one. In realistic running, although the humidification is stable, dynamic load results in humidity fluctuating seriously and induces mechanical degradation [8]. There exist different opinions about the relationship between humidity and PEM decay, some researchers believe low humidity will cause more seriously PEM damage compare with high humidity [9–13]. That's said, on the one hand, under low humidification conditions, MEA will produce a humidity difference between inlet with low water content and outlet area with high water content, which is further exacerbated by different proton conductivity under different humidity [14]. Eventually, PEM in inlet area will dry out and tend to produce cracks. On the other hand, dehydration induces the

* Corresponding authors.
E-mail addresses: gengjt@dicp.ac.cn (J. Geng), zhgshao@dicp.ac.cn (Z. Shao).

https://doi.org/10.1016/j.cjche.2022.07.035
1004-9541/

increase of H_2 crossover and accelerates the chemical degradation of PEMFCs [15,16]. Others consider high humidification will cause more seriously PEM damage because of swelling stress [17,18]. Young's modulus, one of the mechanical properties, decreases as humidity increase, meaning that membrane's mechanical performance decrease as humidity increase [19]. Higher relative humidity (RH) induces larger swelling stress and shorter lifetime [20]. Therefore, it is necessary to explore further relationship between humidity and PEM decay. Despite the controversy about the impact of RH on PEM, most researchers agree that chemical and mechanical decay occur simultaneously in realistic operation. However, there are less investigations about the synergy of these two degradation mechanisms.

CL degradation, the main reason for performance decay [3,21], is characterized by complexity and simultaneity of attenuation modes including Pt coarsening, Pt dissolution, carbon corrosion and ionomer loss for Pt/C [8,22,23]. Humidity plays an important role in these degradation mechanisms. Due to higher potentials causing more oxidization, Pt electrocatalysts tend to attenuate on the cathode side, rather than the anode [24]. Therefore, researches on RH and CL are focus more on the cathode. Firstly, dissolution and coarsening of platinum are one of main reasons for CL performance loss [25,26]. Repeated oxidation and reduction of Pt result in Pt dissolution. When the potential sweeps from the LPL (low potential limit) to the UPL (upper potential limit), Pt dissolution occurs during this process at a low rate. Pt surface forms Pt oxidation whose coverage increases as the dwell time increases at UPL. As the potential is swept down to the LPL, Pt oxidation is reduced as it reacts with protons to form dissolved Pt and water [27]. Dissolved Pt can induce two different pathways of ECSA (electrochemical active surface area) loss. In the first way, when the LPL is above 0.6 V, some Pt^{2+} diffuse through the ionomer phase towards the membrane and are reduced in the membrane by the crossover hydrogen, which results in a Pt band formation at the membrane-cathode interface [28]. In the second pathway, since the voltage is below 0.6 V, Pt^{2+} redeposit on nearby larger Pt nanoparticles, thereby increasing the Pt particle size [27]. This is known as electrochemical Ostwald ripening. In oxidized process, water is one of the reactants. Takei and Uchida [25] indicated that the dissolution of platinum is accelerated in higher RH. In addition, Pt dissolution seems to be the controlling step for Ostwald ripening [26], high humidity will cause larger agglomeration of Pt particles [25,28]. Secondly, during RH cycling, ionomer in CL is prone to cluster [29]. In addition, ionomer volume changing with RH, causing shrinking-swelling cycle [30]. These cause ionomer redistribution unevenly and Pt particles uncovered or overcovered, uncovered Pt surfaces are not accessible to protons, inducing three-phase interface loss and decrease in ECSA. Conversely, agglomerated ionomer hinders the oxygens from reaching the over-covered Pt surface, resulting in a higher mass transfer resistance [31]. Thirdly, carbon corrosion happens under high cathode potential induced by startup-shutdown or fuel starvation [8]. Kwon *et al.* [32] found compared with 30% humidification, structural deterioration of supporting carbon is more serious due to the COR (carbon oxidation reaction) at saturated humidification.

Even if there are many researches to report the humidity effects on degradation, the studies about humidity effects on the whole MEA is less. In the process of long term operation, humidity impacts obviously on the above two components [9]. Moreover, it is different for the relationship between humidity and decays of MEA components. Therefore, humidification can be considered as one of the optimizable parameters to coordinate MEA attenuations and achieve the durability targets [33]. If humidification is optimized, attenuation can also be partly alleviated. It is of great significance to study the influence of humidification on PEMFC attenuation.

Real vehicle drive-cycles, ASTs (accelerated stress tests) [8], and simulating automotive protocols [34] are the main methods to access MEA decay running in light duty vehicle. A real vehicle drive-cycle needs to operate 5000 h for automotive applications according to DOE (department of energy) durability targets [35], which is time-consuming and costly. ASTs are applied to research rapidly the attenuation of MEA components. However, the AST method usually explores only one attenuation of one particular component. Therefore, it is hard to reflect the true natures of PEMFC operated in realistic conditions characterized by complexity and simultaneity. Therefore, developing the test protocols which combine rapidity and validity will be helpful to the research of degradation. The simulating automotive protocols can satisfy the demands. A comprehensive automotive protocol should consist of typical operating conditions [34], whose selection and proportion in the whole duration should follow realistic situation and the purposes of testing.

In this paper, a light duty automotive protocol with frequent dynamic load was designed to simulate the degradation in realistic running. Single cells are operated under this protocol in different humidification, including RH 100%, RH 80%, RH 64%, and RH 40%, RH 10%, to analyze the effects of RH to MEA. PEM decay is characterized by LSV (linear sweep voltammetry), IC (ion chromatography), NMR (nuclear magnetic resonance), and SEM (scan electron microscope) to propose a degradation mechanism under this protocol. CL degradation is accessed by CV (cyclic voltammetry), EIS (electrochemical impedance spectroscopy), XRF (X-ray fluorescence), XRD (X-ray diffraction), TEM (transmission electron microscope), XPS (X-ray photoelectron spectroscopy) to understand the relationship between RH and CL decay. Eventually, according to the impact of RH on PEM and CL, a strategy about humidification is proposed to partly mitigate attenuation.

2. Experimental

2.1. Preparation of MEA

The MEA was fabricated *via* catalyst coated membrane (CCM) and GDL purchased from Mingtian Hydrogen Energy Technology. The CCM was prepared *via* spraying catalyst ink onto Nafion® NR211 (DuPont), and the catalyst ink was composed of commercial Pt/C catalyst (70% (mass) Pt content, Johnson Matthey) and ionomer dispersion (Nafion D520, Du Pont). The GDL was made up of Carbon paper (Toray TGP-H-060) and MPL (microporous layer). The effective electrode area was 25 cm^2 (5 cm × 5 cm). The loading of Pt catalysts for cathode and anode was 0.4 $mg{\cdot}cm^{-2}$ and 0.2 $mg{\cdot}cm^{-2}$ respectively. The fuel cell fixture was fastened with an assembly torque of 5 N·m. After assembly, the single cell was activated at 0.6 V for 6 h.

2.2. Test conditions

Air was fed into cathode and H_2 was fed into anode. The back pressure and temperature of fuel cell were maintained constantly at 0.1 MPa, 70 ℃. The temperature of humidifier was set as 70 °C, 65 °C, 60 °C, and 50 °C, 25 °C, relative humidity was about 100%, 80%, 64%, 40%, 10%, respectively. Reactants were stoichiometrically controlled at 1.5 and 2.5 respectively. There is a minimum gas limit for the test bench of fuel cell, 0.1 $L{\cdot}min^{-1}$ for anode and 0.2 $L{\cdot}min^{-1}$ for cathode. Gases inlet pipes were heated 5 ℃ above cell operating temperature.

A simulating automotive protocol was designed as shown in Fig. 1 and Table 1, characterized by frequent change, spending only 3 min each cycle, in which many conditions were included, such as OCV (open circuit voltage), idling, dynamic load, rated load, over

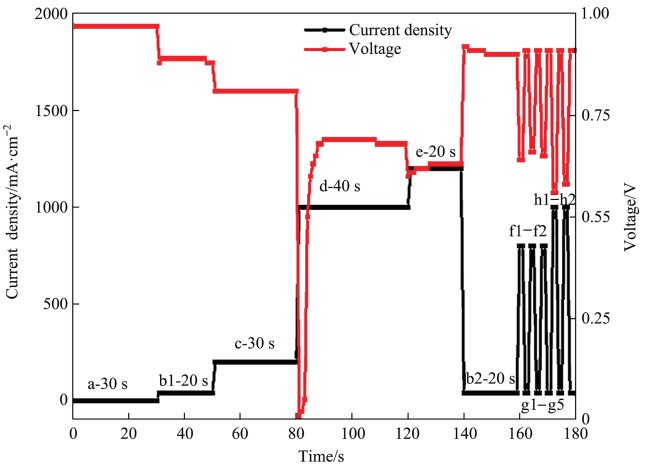

Fig. 1. Protocol for light duty automotive.

load. In addition, it included two phases (phase I and phase II), both characterized by frequent load changing between idle and rated load, and phase II fluctuated every-two seconds.

2.3. Electrochemical testing

Electrochemical testing included electrochemical impedance spectroscopy (EIS), cyclic voltammetry (CV) and linear sweep voltammetry (LSV), measured every 13 h. After polarization curves measurement, EIS were carried out using an electrochemical workstation (GAMRY INTERFACE 5000E) at galvanostatic mode under a constant current of 1000 mA·cm^{-2} with a frequency range between 10 kHz and 0.1 Hz. A sine wave distortion of 250 mA amplitude was applied. CV measurement was performed using the electrochemical workstation with feeding N_2 into cathode and H_2 into anode. The potential was scanned at a rate of 50 mV·s^{-1} from 0.05 V to 1.2 V. For LSV, the scan range is 0.05 V to 0.45 V with 2 mV·s^{-1} rate.

2.4. Structural characterizations

Measurement of Pt loading on cathode of BOL and EOL were performed through XRF using a BRUKER M4 TORNADO. XRD patterns of cathode for studying the crystallite size of Pt nanoparticles were collected through an Empyrean-100 X-ray diffractometer. IC using a Thermo Fisher ICS-1100 was applied to analyst fluorine content in water produced in cathode. A TEM (JEOL JEM-2100, 200 kV) was employed to investigate the BOL and EOL particle size distributions. A SEM (JEOL JSM-IT300, 10 kV) was applied to obtain the thickness of PEM. NMR (BRUKER AVANCE III 600 MHz) was employed to study the PEM chain scission. XPS (Thermofisher Excalab 250 Xi) was applied to analyst the amount and valence of elements in CCL (cathode catalyst layer). Universal Testing Machine (SANS CMT4503) were carried out on PEM mechanical properties.

3. Results and Discussion

The dynamic load between OCV and rated power is regarded as a disastrous damage for MEA [8]. For the automotive protocol, from stage a to stage b2, the voltage changes from OCV to ~ 0.6 V, and then back to ~ 0.9 V in 3 min. The protocol could result in fluctuation of water content in MEA, oxidation and reduction in CL, and chemical radicals during OCV, challenging the mechanical properties of membrane, the stability of CL, and the durability of MEA. In the test of different humidity, the degradations induced by the protocol are obviously affected by RH. On the one hand, Fig. 2(a), (b) and Fig. S1(a)–(c) (in Supplementary Material) shows polarization curves under different RHs and Fig. 2(c) presents the attenuation of potential under 800 mA·cm^{-2} over operation time at RH 100%, RH 80%, RH 64%, RH 40%, RH 10%, indicating that CL attenuation is taking place. The extent of CL degradation as a consequence of RH will be investigated in Section 3.1. On the other hand, when H_2 crossover current density calculated from LSV is over 25 mA·cm^{-2}, PEM will be regarded as appearing pinholes or cracks and stop running. Hydrogen crossover current density calculated from LSV under different operation time shows in Fig. 2(d), it shows a different trend under various RH, indicating that PEM attenuation is affected by RH. The relationship of generating pinholes in membrane with humidity will be investigated in Section 3.2.

3.1. The influence of humidity on CL

The CL loss, to be exact, is not caused by one reason, but following four reasons: (i) electronic connectivity loss due to carbon support corrosion, (ii) catalyst loss due to dissolution or detachment, and (iii) physical surface area loss due to particles growth, (iv) proton connectivity loss due to ionomer/catalyst interface loss [8,22,23]. These four processes occur in parallel and result in CL loss. In order to evaluate the effect of humidity to CL degradation, two single cells operated in RH 64% and RH 10% are presented here owing to the same durability time.

Firstly, CV is measured at various operation time shown in Fig. S2. The normalized ECSA, calculated from CV, changes under two RH shown in Fig. 3(a). At EOL (end of life), a 57.5% ECSA attenuation under RH 64% and a 41.7% decay under RH 10% were observed, which is consistent with the change of R-ct (charge transfer resistance) presented in Fig. 4(c), in which the R-ct displays a more outstanding increase in RH 64%. The discrepancy in ECSA indicates that the sum of carbon corrosion, Pt loss and Pt growth is more pronounced in RH 64% than RH 10%. However, the whole degradation can be characterized by voltage drop in Fig. 2(c), the decay rate is 103 μV·h^{-1}, 103 μV·h^{-1}, 136 μV·h^{-1}, 210 μV·h^{-1} and 357 μV·h^{-1} for RH 100%, RH 80%, RH 64%, RH 40%, and RH 10%, respectively. The degradation rate increases with RH decrease. Therefore, we suggest a relatively high humidity to improve the initial performance

Table 1
Illustration for each stage of light duty automotive protocol.

Stage	Current density/mA·cm^{-2}	Initial voltage/V	(I/I_{max})/%	Duration/s	Proportion/%	Condition
a	0	0.97	0	30	16.7	OCV
b(1,2)	1	0.89	4	40	22.2	Idling
c	5	0.81	20	30	16.7	Low load
d	25	0.68	100	40	22.2	Rated load
e	30	0.63	120	20	11.1	Over load
f(1−3)	20	0.64	80	6	11.1	Dynamic load
g(1−5)	1	0.91	4	10		
h(1,2)	25	0.53	100	4		

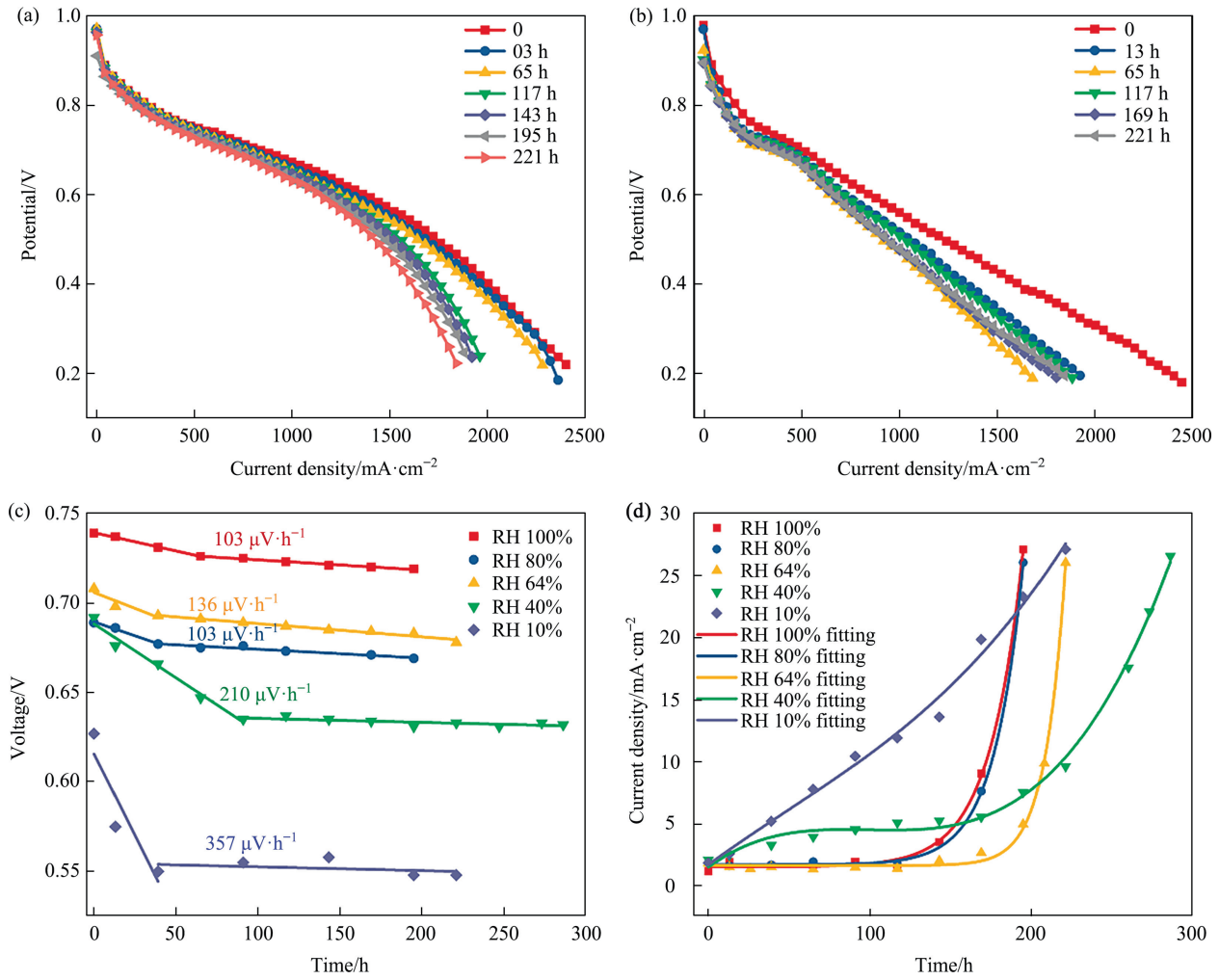

Fig. 2. (a) Polarization curves *versus* operation time in RH 64%, (b) polarization curves *versus* operation time in RH 10% (polarization curves under other RHs shown in Fig. S1 (a)–(c)), (c) Potential change under 800 mA·cm^{-2} over operation time under the five RH, (d) H_2 crossover current density *versus* operation time under different RHs.

and mitigate the whole decay. In addition, the performance loss is more pronounced in RH 10% than RH 64%, indicating the ionomer loss is more remarkable in RH 10%, and its decay affects performance seriously in low humidity, which will be proved by XPS. To explore the relationship RH and CL decay, the specific reason for the CL loss needs to be investigated further. The above four mechanisms can be analyzed by characterization techniques, including XRF, XRD, TEM, XPS, and electrochemical measurement. The μ-XRF was used to measure the Pt loading before and after the simulating automotive protocol; EIS was used to calculate the change of DLC (double-layer capacitance), to evaluate carbon corrosion; particles coarsening was investigated by XRD and TEM; ionomer/catalyst interface loss was analyzed by XPS.

Secondly, Platinum load decrease is both observed. It differs as the change of RH. Fig. 3(b) shows the Pt loss under RH 64% and 10%. There exists more Pt loss in RH 10%. For the automotive protocol, the fuel cell experiences an oxidation and reduction process for each cycle. Potential reaches 0.97 V at BOL (begin of life) during the OCV, Pt surface is oxidized and forms Pt oxidation [27]. As the potential is swept down to the stage d and stage e, Pt oxidation is reduced and Pt dissolves with the oxygen atom escaping from Pt surface. The reduction potential is the major distinction is in these two RH under the same protocol. It is above 0.6 V in RH 64% while it is 0.4–0.5 V in RH 10%, leading to the different extent of oxygen escaping and Pt loss which are accelerated by the low reduction potential. In addition, XPS spectra, presented in Fig. 3(c), is used to analyst atomic concentrations changing of CCL surface area before and after the automotive condition at RH 60% and 10%. Fig. 3(d) shows the contents of F obtained from the full spectrum of XPS. It is obvious of the contents change for BOL and EOL due to the degradation which is different for RH 64% and 10%. The fluorine signal displays no significant changes in RH 64% compared with BOL, while it decreases pronounced in RH 10%, meaning that there is more ionomer loss in RH 10% in cathodal CL. The volume of ionomer reduces with humidity decrease due to ionomer loss, resulting in increased catalyst surface exposure. The Pt dissolution increase with the increase of the catalyst surface exposure [36]. Therefore, Pt loss is more pronounced in low humidity. The reason for ionomer loss is similar with the PEM degradation illustrated in Section 3.2.

Thirdly, support carbon corrosion can be estimated by the change of DLC in the absence of any Faradaic processes [22,37]. Fig. 4(a) and Fig. S3 present the Nyquist plot at various operating time in RH 64% and RH 10%. The impedance arcs both increase with the operation time, meaning that a performance loss exists in MEA. The equivalent circuit is designed as shown in Fig. 4(a) inset. The DLC change calculated by EIS fitting shown in Fig. 4(d), noticeably decreases for RH 64% compared with RH 10%, indicating that high RH can lead to more carbon corrosion. In this paper, the carbon corrosion results from the fuel starvation. The supply of H_2 and

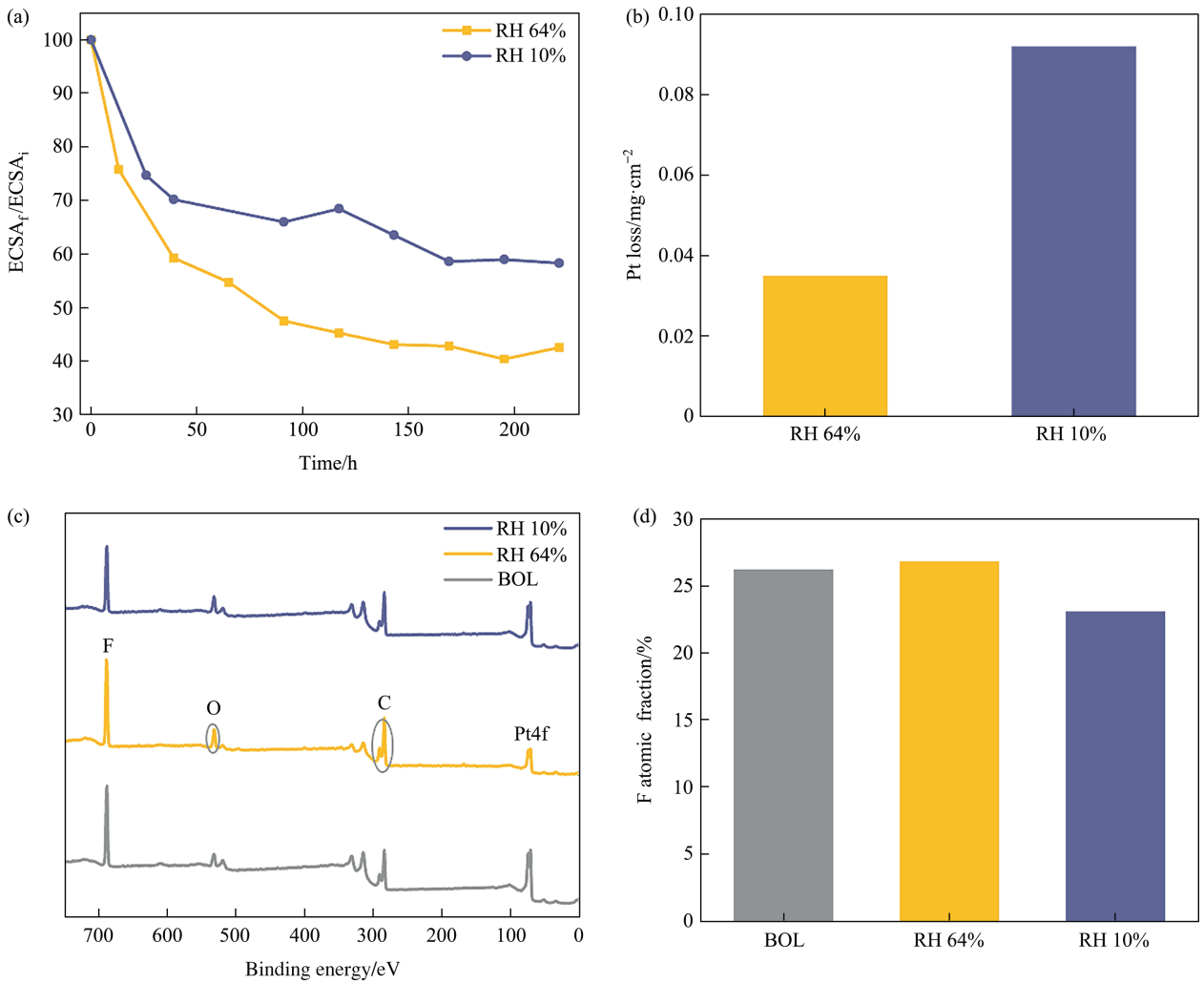

Fig. 3. (a) ECSA *versus* operation time during automotive protocol in RH 64%, and RH 10%, (b) Pt loss under RH 64% and RH 10%, (c) XPS survey spectrum of the CCL before and after the automotive condition at RH 64% and 10%, (d) Fluoride atomic fraction in CCL based on the XPS spectra.

air lags behind the load increase under automotive protocol; therefore, gas starvation occurs owing to the late gas supply controlled by stoichiometric, and the extent of starvation is more remarkable with the more increase of load. There are many the load-up process in Fig. 1, especially in stage c to stage d and phase II. The current of the former increases from 5 A to 25 A, and the current of the later fluctuates between 1 A and 20–25 A. The voltage drops sharply from 0.81 V to 0 V in stage c to stage d, and it is back to a normal level after 4–8 s at BOL. With the exacerbation of decays, the starvation time will be extended. The fuel starvation in anode leads to the carbon corrosion in cathode and accelerates fuel cell aging. Therefore, carbon corrosion occurs mainly in the starvation time. In addition, carbon corrosion appears more pronounced decay in RH 64% presented in Fig. 4(d) inset. A 37.98% DLC loss is observed in RH 64% as compared with 23.01% loss in RH 10%. This phenomenon can be explained from the mechanism of carbon corrosion. As fuel starvation happens, the reaction in cathode will be governed by the COR or OER (oxygen evolution reaction). One of the reactants is water in COR, accordingly, more water can accelerate the COR or OER rate. Hence the carbon corrosion shows a relatively high degradation rate in RH 64%.

Lastly, catalyst coarsening occurs easily in this automotive protocol. Pt coarsening was elaborated systematically by XRD and TEM, presented in Fig. 5. Mean Diameter for BOL, RH 64% and RH 10% is 2.1 nm, 6.7 nm, 5.3 nm, respectively, calculated by ImageJ of TEM images, 4.8 nm, 10.7 nm, 8.8 nm estimated by Scherer formula from the peak broadening of the Pt(111) and Pt(200), the fitting results shows in Table S2. These results both showed a dramatical Pt aggregation was observed after the automotive protocol at RH 64% and RH 10%. In addition, Pt growth at RH 64% is more significant. Electrochemistry Ostwald ripening is a generally accepted mechanism to Pt particles growth. Virkar *et al.* [38] presented the mechanism of catalyst particle growth in PEMFCs as Ostwald ripening. Pt dissolves from small particles into the ionomer while electrons transport through the carbon support and then Pt deposits on big particles to reduce particle surface energy, hence the average particle size increases. Therefore, there are three factors affecting the Ostwald ripening, including Pt dissolution, carbon support, and ionomer. The ionic conductivity of the ionomer is an important factor in electrochemical Ostwald ripening and particle growth. Water content is a significant contributor to the ionic conductivity of the ionomer [25,39]. The Pt ion transport in the ionomer will decrease and even be blocked with the shrinking and decay of ionic channel networks due to the low humidity and chemical decay. Because the rate of Pt ion transport is slower in RH 10%, the redeposition of Pt was inhibited.

To sum up, the automotive protocol is characterized by dynamic load, inducing repeated oxidation and reduction cycles, air starvation, and OCV. After the protocol, four mechanisms about CL degradation, including Pt dissolution, ionomer decay, carbon corrosion and Pt growth, are observed in this section. The extent of degradation is a pronounced difference in various humidity.

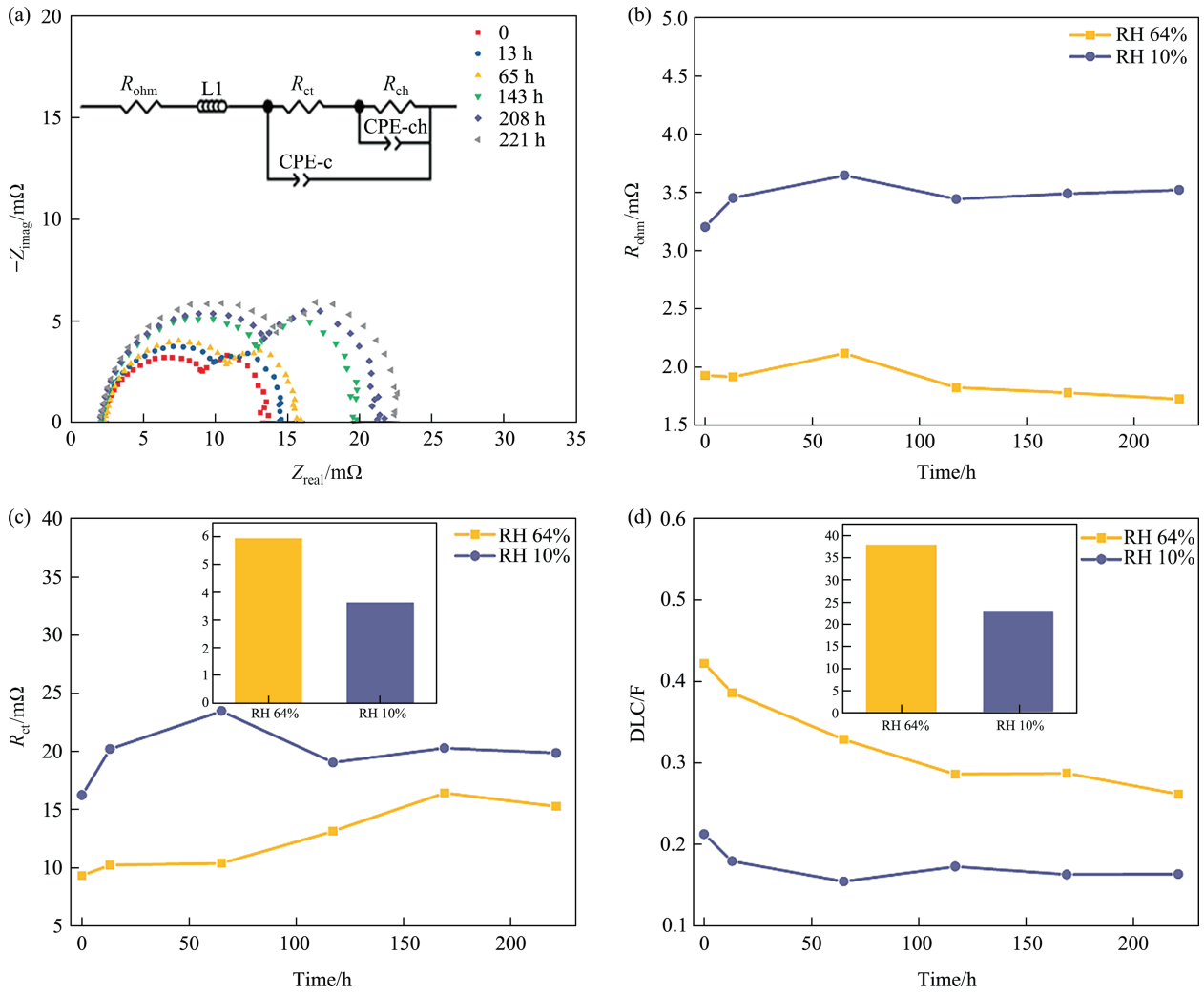

Fig. 4. (a) Nyquist plot at various operating time during simulating automotive protocol under RH 64%, (b) R_{ohm}, (c) R_{ct}, (d) DLC changing *versus* operation time, (a inset) the equivalent circuit for these single fuel cells, (c inset) the comparison of R_{ct} increase for RH 64% and RH 10%, (d inset) the comparison of DLC loss for RH 64% and RH 10%.

Ionomer degradation occurs more severely in low humidity with high chemical decay induced by hydrogen crossover, it is the main reason for performance loss of fuel cell in low humidity. The Pt loss is more pronounced in RH 10%, which is likely to be due to the lower reduction potential and higher catalyst surface exposure causing by ionomer degradation. Since the water participates in the reactions of carbon corrosion, carbon corrosion is accelerated by higher water content in RH 64%. Pt growth is as the consequence of serious Ostwald ripening, which maybe owing to the high-speed ion transport channels in RH 64% as a consequence of more water. In addition, the degradation rate increases with RH decrease shown in Fig. 2(c), meaning that the sum of these decays attenuates CL performance is more pronounced in low humidity. Consequently, operating in a relative high humidity can help reduce CL degradations. However, flooding results in outstanding voltage drop in high humidity, causing a bad MEA performance. Therefore, a relative high humidity, like RH 64%, is benefit for improving the initial performance and reduce CL performance loss under automotive protocol.

3.2. The influence of humidity on PEM

In this paper, PEM appears pinholes or cracks leading to hydrogen crossover reaching 25 mA·cm^{-2} after the single fuel cells have been operated for 189 h at RH 100% and RH 80%, 221 h at RH 64%, 286 h at RH 40%, and 221 h at RH 10%, indicating that a high and low humidity are both against the longer durability for PEM and only the modest RH, like RH 40%, can mitigate the generation of pinholes. The reason of generating pinholes in PEM will be discussed in the next four aspects.

Firstly, the state of PEM can be demonstrated by the change of H_2 crossover versus operation time, shown in Fig. 2(d). The change shows a pronounced difference under these five RH. The change can be divided into two stages in high humidity including RH 100%, RH 80% and RH 64%. In the early stage, H_2 crossover anchors at level below 2 mA·cm^{-2}, indicating that membranes are in good condition, but it does not mean that membrane attenuation has not occurred. PEM decay, including mechanical and chemical degradation, is always accumulated, just not reflected in LSV at this period. However, in the later period, H_2 crossover increases rapidly causing the PEM failure, as a consequence of cracks and pinholes in PEM. These defects are likely to be due to the accumulation of mechanical decay by humidity cycle and chemical decay by H_2 crossover in the early stage. The change shows a similar trend under RH 40%; however, the difference is a more pronounced H_2 crossover reaching 5 mA·cm^{-2} in the early stage. The condition means that more chemical degradation caused by H_2 crossover happens in RH 40%. It is unexpected for PEM under RH 40% to achieve the slowest degradation rate for pinholes between the five RH. There exists the most obviously distinction between RH 10%

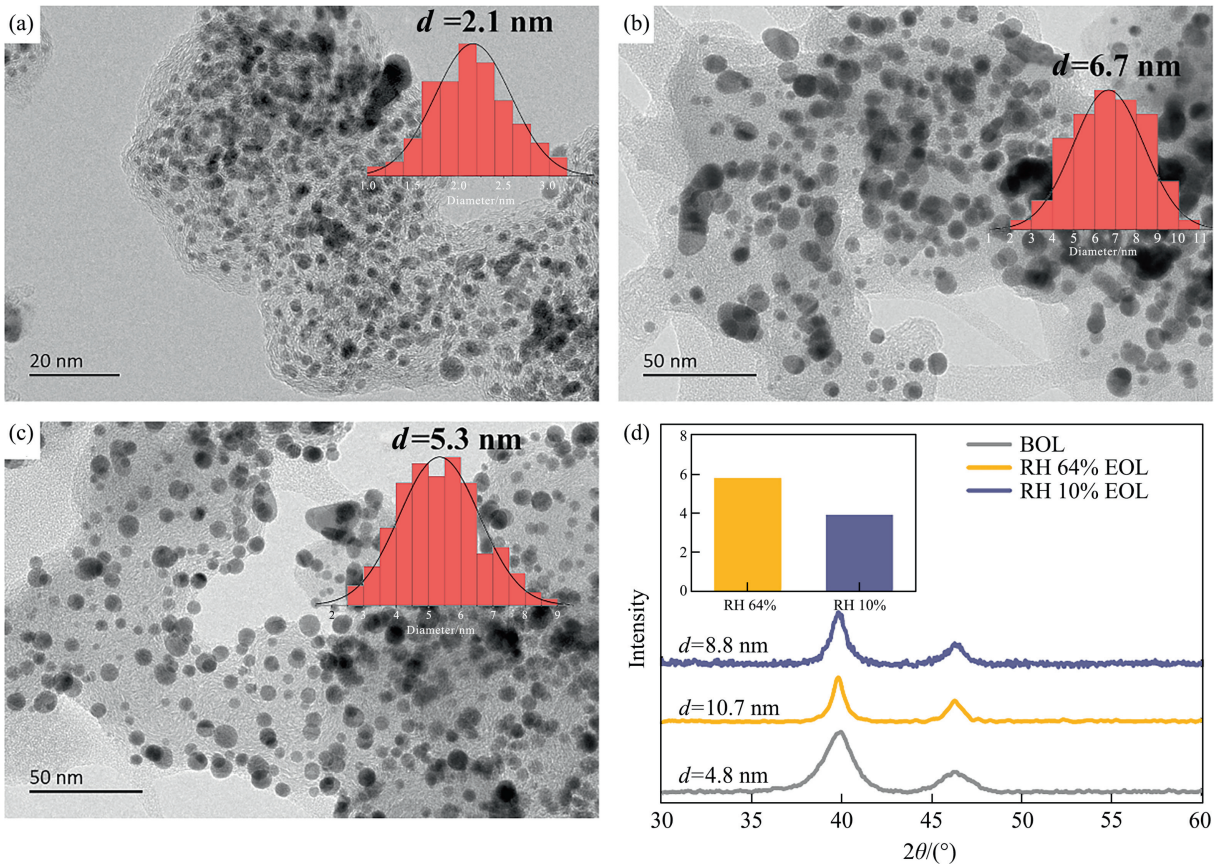

Fig. 5. TEM images and particle size histograms of the cathode CL (a) before of life, after automotive protocol in (b) RH 64 %, (c) RH 10 %, (d) XRD patterns of the cathode CL before and after simulating automotive protocol in these five RHs.

and other RH. The H_2 crossover does not exist the early stage, and keeps increasing during the whole life. These results indicate the RH can cause the discrepancy of H_2 crossover which is more severe in low humidity. However, the PEM in RH 40% with more H_2 crossover than high humidity presents the slowest degradation rate for pinholes, meaning that chemical attenuation caused by H_2 crossover affects the PEM decay but it dominates the membrane decay only in an extreme low humidity.

Secondly, the principal evidence for chemical degradation is fluoride release and membrane thinning [40]. The fluoride originates from the breaks of PSFA, attacked by free radicals generated from chemical reaction. To analyze chemical attenuation of PEM, the cumulative fluoride loss collected in the effluent water is illustrated in Fig. 6(a) under these five RH. Fluoride concentration at RH 10% and RH 40% is always higher than other RHs before 169 h, demonstrating that low humidity induces a more serious chain scission and fluoride loss. In addition, membrane thinning is another visible phenomenon associated with chemical attenuation. Fig. 7(a)–(f) shows SEM images before and after automotive protocol under these five RH. The average thickness of membrane shows in Fig. S4. Compared with the CCM at BOL, the membrane thickness both decreases after the automotive protocol, and the membranes under low RH appear a more severe thickness loss. PEM is a porous material, and the porosity of the membrane decreases with RH increase, resulting in reduced gas permeation [41]. Gas crossover is the root of the generation of free radicals [42]. Consequently, more crossover oxygen reacts with hydrogen to produce free radicals with less water in low humidity, leading to more thickness loss of membranes in RH 40% and RH 10%. The two phenomena both demonstrate chemical attenuation is more serious in low humidity.

Noticeably, membranes in high RH, including RH 100%, RH 80%, RH 64%, appear non-uniformity thickness compare with membranes in low RH. There exists a $\sim$ 15 μm difference between the thickest and the thinnest part, and the thinnest place shows only 13.9 μm in RH 100% shown in Fig. 7(b), which could be caused by the stress cycling along the in-plane direction. For automotive protocol, low load stages occupy $\sim$ 55.5% of the whole protocol, high load stages dominate 33.3%. Dynamic load in the automotive protocol induces humidity cycle so that PEM experiences swelling and shrinking cycle in response to the humidity change. Some places become thicker than initial and some places become thinner due to the constant volume, meaning the non-uniformity thickness, indicating mechanical degradation happens more seriously in high humidity. The in-plane swelling stress is the major stress during hydration and dehydration cycles, which is the main reason for PEM mechanical degradation. For PFSA membrane, 30% humidify is regarded as no swelling strains in plane direction and the stress increase with the raise of humidity [17,18]. Therefore, PEM in high humidity will experience more mechanical stress.

Thirdly, in order to evaluate mechanical properties, the tensile traction tests are carried out before and after the protocol. The stress–strain curves are shown in Fig. S5. The mechanical properties display a pronounced changes compared with the BOL sample. Fig. 6(b) shows changes in the elongation at break of the membranes, used to assess the ductility of the PEM. The smaller elongation is observed under RH 100%, RH 80%, meaning that the polymer becomes less ductile or more brittle after a mechanical stress under high RH protocol, causing a faster rate for generating pinholes. However, PEMs display a greater elongation at break in RH 40% and RH 10%, indicating that the ductility is better and mechanical stress impacts slightly on PEM in low humidity.

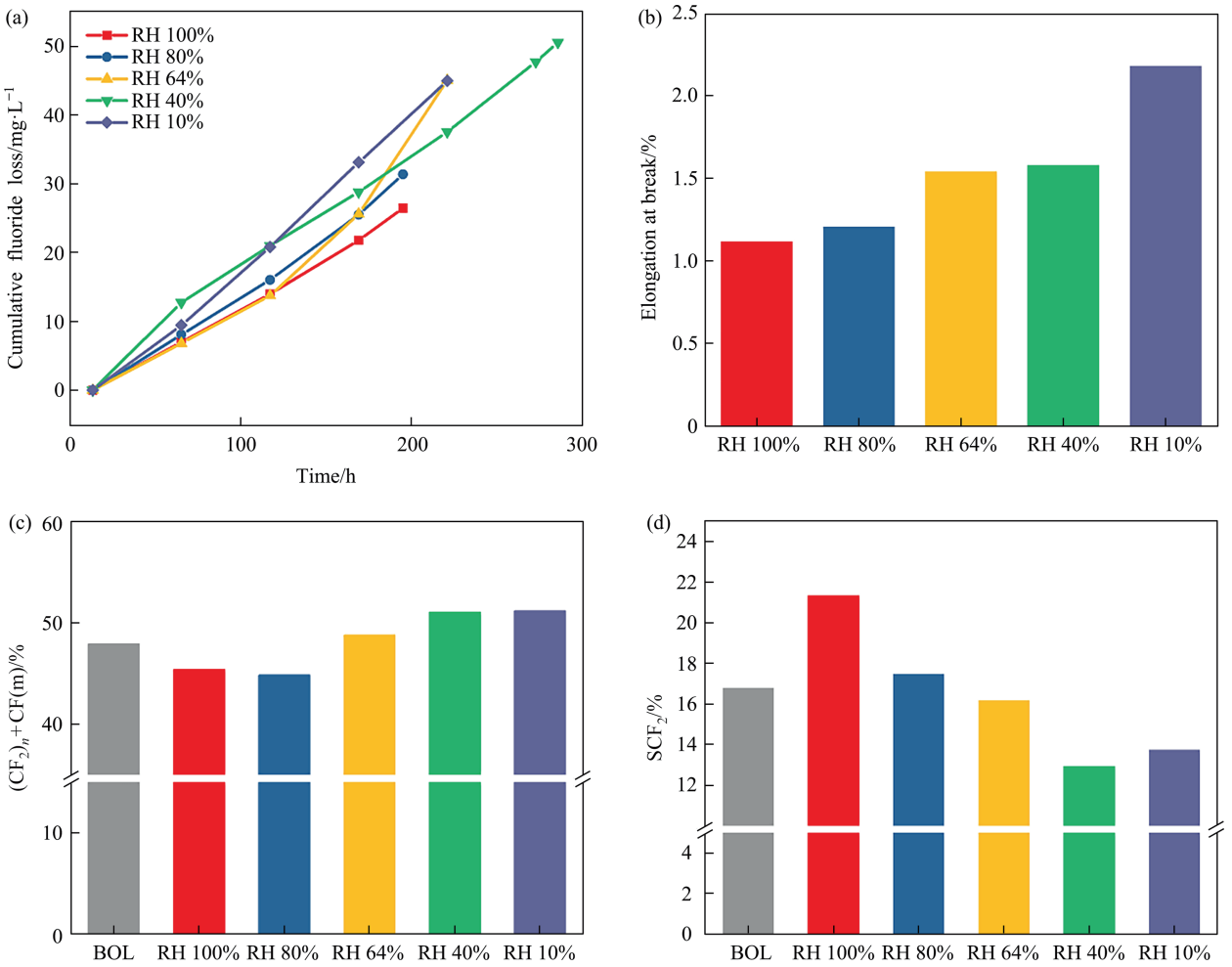

Fig. 6. (a) The cumulative fluoride concentration in drain water *versus* operation time under these five RH, (b) Elongation per thickness after test under these five RH. (c) CF (main chain), $(CF_2)_n$ in membrane before and after test under these five RH, (d) SCF_2 in membrane before and after test under these five RH.

Therefore, the SEM images and tensile tests support that the mechanical degradation happens severely in high humidity, and mechanical stress along in-plane direction maybe the mainly reason for pinholes in high humidity.

In addition, the mechanical decay causes a faster degradation rate for pinholes than chemical decay according to the time of hydrogen crossover reaching 25 mA·cm^{-2}. The mechanical damage to PEM leads to extremely thin thickness in some area, resulting in generation of pinhole in these thinner areas and the hydrogen crossover current density reaching 25 mA·cm^{-2} earlier.

Lastly, NMR has been carried out to further support the chemical and mechanical degradation. Fig. S6 and Fig. S7 present the ^{19}F NMR spectra of PEM, separated and assigned according to the work of Ghassemzadeh and Holdcroft [43]. There are five peaks, including CF (main chain), $(CF_2)_n$, CF (side chain), SCF_2, OCF_2, and CF_3. The main chain determines the mechanical properties, and the side chain determines proton conductivity *via* a terminal sulfonic acid group [44]. The first two fluorides are associated with main chain, and they are compared before and after automotive protocol under these five RH shown in Fig. 6(c). The membrane shows a more serious main chain scission at high humidity, including RH 100%, RH 80%, and RH 64%, and it presents a less amount of main chain under high humidity compared with low humidity, indicating that the mechanical properties of PEM are poor in RH 100%, RH 80% and RH 64%, conforming that the mechanical degradation happened more severe in high humidity, which is in accordance with the conclusion of Lu *et al.* [19], Kusoglu *et al.* [20]. The SCF_2 is associated with proton conductivity, and the amount of SCF_2 under these five RH shows in Fig. 6(d). it presents a less amount of SCF_2 under RH 40% and RH 10% compared with high humidity, indicating that the chemical properties of PEM are poor in RH 40% and RH 10%, supported by the R_{ohm} change with time shown in Fig. 4(b). The R_{ohm} consists mainly of membrane resistance. It slightly increases from 3.2 mΩ·cm^{-2} to 3.5 mΩ·cm^{-2} in RH 10%, indicating that the proton conductivity decreases as a consequence of PEM chemical decay in RH 10%, confirming the SCF_2 loss in low humidity.

To sum up, the pinholes in PEM originate mainly from mechanical and chemical damages in this paper, and they occur simultaneously. The proportion of the two degradations is different in various RH. The more H_2 crossover, the worse fluoride loss, and the thinner membrane thickness indicate more chemical degradation in low humidity, including RH 40% and 10% under automotive protocol. Chemical attenuation occurs more violently for RH 10%, which is consistent with the results of Kwon *et al.* [15]. The non-uniformity thickness and bad mechanical properties are more likely to be due to mechanical stress in plane direction in high humidity, including RH 100%, RH 80% and 64% under automotive protocol. The experiment of Lu *et al.* [19] showed a similar results. However, these two degradations are weakened in 40%. In addition, the PEM displays a more pronounced hydrogen crossover in the early stage for RH 40%, meaning more chemical degradation happens. However, the chemical decay does not result directly in pinholes generation, speculating that chemical decay is an accumulated process with a lower rate to attenuates PEM thickness.

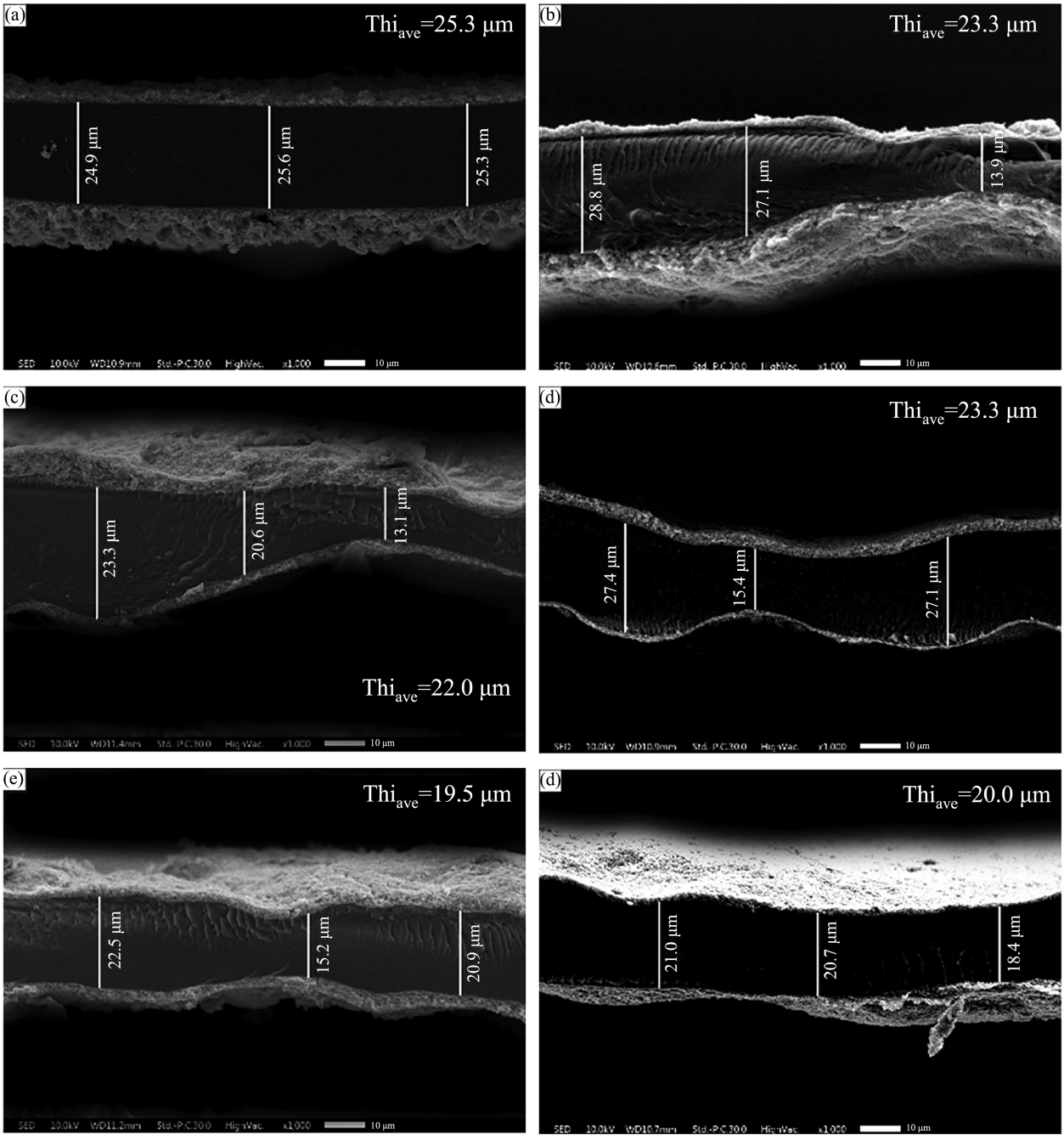

Fig. 7. SEM images of CCM under (a) BOL, (b) RH 100 %, (c) RH 80 %, (d) RH 64 %, (e) RH 40 %, (f) RH 10 %.

4. Conclusions

To promote the commercialization of PEMFCs in automotive applications, the PEM and CL degradations are investigated under the automotive protocol as the function of different humidity, including RH 100%, RH 80%, RH 64%, RH 40%, RH 10%. Therefore, a suitable humidity can be proposed to mitigate the decay of MEA under automotive protocol. The effects of humidity to MEA can be discussed in two aspects. On the one hand, the decay rate decreases with RH increase for CL under automotive protocol. Therefore, high RH be conducive to slow the degradation in CL. In addition, four degradation mechanisms, including Pt dissolution, Pt coarsening, carbon corrosion and ionomer degradation, are different in high and low humidity. Pt coarsening and carbon corrosion maybe accelerated by higher water content inducing the more performance loss for RH 64%. Ionomer degradation and Pt dissolution is enhanced in low humidity for RH 10%. Pt dissolution maybe caused by increased catalyst surface exposure induced by ionomer degradation. On the other hand, chemical and mechanical degradation is the mainly reasons for PEM generating pinholes. Chemical factors are the main reason for more fluoride loss and less membrane thickness, observed seriously in RH 10% under automotive protocol, and mechanical factors are more likely to lead to the non-uniformly thickness and bad elongation at break, noticed notably in RH 100%, RH 80%, and RH 64% under automotive protocol. These two degradations show a moderate level in RH 40% under automotive protocol. Overall, to slow the CL attenuation and improve the initial performance, PEMFCs should be operated in RH 64%. To extend PEM durability, it is desirable to operate PEMFC at RH 40%. Combining the CL and

PEM decay, the RH range from 64% to 40% is suggested to automotive protocol.

Declaration of Competing Interest

The authors declare that they have no known competing financial interests or personal relationships that could have appeared to influence the work reported in this paper.

Acknowledgements

This research is supported by the National Key Research and Development Program of China (2018YFB1502502), the National Natural Science Foundation of China (22179127).

Supplementary Material

Supplementary material to this article can be found online at https://doi.org/10.1016/j.cjche.2022.07.035.

References

[1] Y. Wang, K.S. Chen, J. Mishler, S.C. Cho, X.C. Adroher, A review of polymer electrolyte membrane fuel cells: Technology, applications, and needs on fundamental research, *Appl. Energy* 88 (2011) 981–1007.
[2] J. Zhao, X. Li, A review of polymer electrolyte membrane fuel cell durability for vehicular applications: Degradation modes and experimental techniques, *Energy Convers. Manage.* 199 (2019) 112022.
[3] X. Zhang, Y.P. Yang, X.Y. Zhang, H.T. Liu, Identification of performance degradations in catalyst layer and gas diffusion layer in proton exchange membrane fuel cells, *J. Power Sources* 449 (2020) 227580.
[4] L. Placca, R. Kouta, Fault tree analysis for PEM fuel cell degradation process modelling, *Int. J. Hydrog. Energy* 36 (19) (2011) 12393–12405.
[5] K. Panha, M. Fowler, X.Z. Yuan, H.J. Wang, Accelerated durability testing *via* reactants relative humidity cycling on PEM fuel cells, *Appl. Energy* 93 (2012) 90–97.
[6] J.F. Wu, X.Z. Yuan, J.J. Martin, H.J. Wang, D.J. Yang, J.L. Qiao, J.X. Ma, Proton exchange membrane fuel cell degradation under close to open-circuit conditions: Part I: *in situ* diagnosis, *J. Power Sources* 195 (4) (2010) 1171–1176.
[7] Q.W. Tang, B. Li, D.J. Yang, P.W. Ming, C.M. Zhang, Y.B. Wang, Review of hydrogen crossover through the polymer electrolyte membrane, *Int. J. Hydrog. Energy* 46 (42) (2021) 22040–22061.
[8] P. Ren, P.C. Pei, Y.H. Li, Z.Y. Wu, D.F. Chen, S.W. Huang, Degradation mechanisms of proton exchange membrane fuel cell under typical automotive operating conditions, *Prog. Energy Combust. Sci.* 80 (2020) 100859.
[9] H. Wang, X.-Z. Yuan, H. Li, Fuel Cell Failure Mode Analysis, CRC Press Boca Raton, FL, USA, 2012.
[10] V.A. Sethuraman, J.W. Weidner, A.T. Haug, L.V. Protsailo, Durability of perfluorosulfonic acid and hydrocarbon membranes: Effect of humidity and temperature, *J. Electrochem. Soc.* 155 (2) (2008) B119.
[11] X.Y. Huang, R. Solasi, Y. Zou, M. Feshler, K. Reifsnider, D. Condit, S. Burlatsky, T. Madden, Mechanical endurance of polymer electrolyte membrane and PEM fuel cell durability, *J. Polym. Sci. B Polym. Phys.* 44 (16) (2006) 2346–2357.
[12] J. Xie, D.L. Wood, D.M. Wayne, T.A. Zawodzinski, P. Atanassov, R.L. Borup, Durability of PEFCs at high humidity conditions, *J. Electrochem. Soc.* 152 (1) (2005) A104.
[13] C. Chen, T.F. Fuller, The effect of humidity on the degradation of Nafion® membrane, *Polym. Degrad. Stab.* 94 (9) (2009) 1436–1447.
[14] D. Garcia-Sanchez, T. Morawietz, P.G. da Rocha, R. Hiesgen, P. Gazdzicki, K.A. Friedrich, Local impact of load cycling on degradation in polymer electrolyte fuel cells, *Appl. Energy* 259 (2020) 114210.
[15] J. Kwon, S. Jo, K.Y. Cho, K. Eom, Deconvolution of the dehydration degradation mechanism in polymer electrolyte membrane fuel cells using electrochemical impedance analysis combined with the transmission line model under low humidity, *J. Power Sources* 473 (2020) 228587.
[16] E. Endoh, S. Terazono, H. Widjaja, Y. Takimoto, Degradation study of MEA for PEMFCs under low humidity conditions, *Electrochem. Solid-State Lett.* 7 (2004) A209.
[17] A. Kusoglu, A.M. Karlsson, M.H. Santare, S. Cleghorn, W.B. Johnson, Mechanical behavior of fuel cell membranes under humidity cycles and effect of swelling anisotropy on the fatigue stresses, *J. Power Sources* 170 (2007) 345–358.
[18] Y.L. Tang, A.M. Karlsson, M.H. Santare, M. Gilbert, S. Cleghorn, W.B. Johnson, An experimental investigation of humidity and temperature effects on the mechanical properties of perfluorosulfonic acid membrane, *Mater. Sci. Eng. A* 425 (1–2) (2006) 297–304.
[19] Z. Lu, M. Lugo, M.H. Santare, A.M. Karlsson, F.C. Busby, P. Walsh, An experimental investigation of strain rate, temperature and humidity effects on the mechanical behavior of a perfluorosulfonic acid membrane, *J. Power Sources* 214 (2012) 130–136.
[20] A. Kusoglu, M.H. Santare, A.M. Karlsson, Aspects of fatigue failure mechanisms in polymer fuel cell membranes, *J. Polym. Sci., Part B: Polym. Phys.* 49 (2011) 1506–1517.
[21] S.S. Zhang, X.Z. Yuan, J.N.C. Hin, H.J. Wang, K.A. Friedrich, M. Schulze, A review of platinum-based catalyst layer degradation in proton exchange membrane fuel cells, *J. Power Sources* 194 (2) (2009) 588–600.
[22] R. Sharma, S.M. Andersen, Quantification on degradation mechanisms of polymer electrolyte membrane fuel cell catalyst layers during an accelerated stress test, *ACS Catal.* 8 (4) (2018) 3424–3434.
[23] R. Sharma, S.M. Andersen, An opinion on catalyst degradation mechanisms during catalyst support focused accelerated stress test (AST) for proton exchange membrane fuel cells (PEMFCs), *Appl. Catal. B Environ.* 239 (2018) 636–643.
[24] R. Borup, J. Meyers, B. Pivovar, Y.S. Kim, R. Mukundan, N. Garland, D. Myers, M. Wilson, F. Garzon, D. Wood, P. Zelenay, K. More, K. Stroh, T. Zawodzinski, J. Boncella, J.E. McGrath, M. Inaba, K. Miyatake, M. Hori, K. Ota, Z. Ogumi, S. Miyata, A. Nishikata, Z. Siroma, Y. Uchimoto, K. Yasuda, K.I. Kimijima, N. Iwashita, Scientific aspects of polymer electrolyte fuel cell durability and degradation, *Chem. Rev.* 107 (10) (2007) 3904–3951.
[25] C. Takei, K. Kakinuma, K. Kawashima, K. Tashiro, M. Watanabe, M. Uchida, Load cycle durability of a graphitized carbon black-supported platinum catalyst in polymer electrolyte fuel cell cathodes, *J. Power Sources* 324 (2016) 729–737.
[26] K. Yu, D.J. Groom, X.P. Wang, Z.W. Yang, M. Gummalla, S.C. Ball, D.J. Myers, P.J. Ferreira, Degradation mechanisms of platinum nanoparticle catalysts in proton exchange membrane fuel cells: The role of particle size, *Chem. Mater.* 26 (19) (2014) 5540–5548.
[27] A.A. Topalov, S. Cherevko, A.R. Zeradjanin, J.C. Meier, I. Katsounaros, K.J.J. Mayrhofer, Towards a comprehensive understanding of platinum dissolution in acidic media, *Chem. Sci.* 5 (2) (2014) 631–638.
[28] K. Khedekar, M. Rezaei Talarposhti, M.M. Besli, S. Kuppan, A. Perego, Y.C. Chen, M. Metzger, S. Stewart, P. Atanassov, N. Tamura, N. Craig, L. Cheng, C.M. Johnston, I.V. Zenyuk, Probing heterogeneous degradation of catalyst in PEM fuel cells under realistic automotive conditions with multi-modal techniques, *Adv. Energy Mater.* 11 (35) (2021) 2101794.
[29] J. Zhao, S. Shahgaldi, X.G. Li, Z.S. Liu, Experimental observations of microstructure changes in the catalyst layers of proton exchange membrane fuel cells under wet-dry cycles, *J. Electrochem. Soc.* 165 (6) (2018) F3337–F3345.
[30] F. Rong, C. Huang, Z.S. Liu, D.T. Song, Q.P. Wang, Microstructure changes in the catalyst layers of PEM fuel cells induced by load cycling: Part II. Simulation and understanding, *J. Power Sources* 175 (2) (2008) 712–723.
[31] S.V. Venkatesan, M. Dutta, E. Kjeang, Mesoscopic degradation effects of voltage cycled cathode catalyst layers in polymer electrolyte fuel cells, *Electrochem. Commun.* 72 (2016) 15–18.
[32] J. Kwon, P. Choi, K. Eom, A comparison study on the carbon corrosion reaction under saturated and low relative humidity conditions *via* transmission line model-based electrochemical impedance analysis, *J. Electrochem. Soc.* 168 (2021) 064515.
[33] D.G. Sanchez, T. Ruiu, I. Biswas, M. Schulze, S. Helmly, K.A. Friedrich, Local impact of humidification on degradation in polymer electrolyte fuel cells, *J. Power Sources* 352 (2017) 42–55.
[34] H.C. Chen, Z. Song, X. Zhao, T. Zhang, P.C. Pei, C. Liang, A review of durability test protocols of the proton exchange membrane fuel cells for vehicle, *Appl. Energy* 224 (2018) 289–299.
[35] J. Kurtz, Fuel cell technology status: Degradation, DOE hydrogen and fuelcells program, in: 2017 Annual Merit Review Proceedings, Washington, D.C., 2019.
[36] S.M. Andersen, L. Grahl-Madsen, Interface contribution to the electrode performance of proton exchange membrane fuel cells - Impact of the ionomer, *Int. J. Hydrog. Energy* 41 (3) (2016) 1892–1901.
[37] O. Reid, F.S. Saleh, E.B. Easton, Determining electrochemically active surface area in PEM fuel cell electrodes with electrochemical impedance spectroscopy and its application to catalyst durability, *Electrochim. Acta* 114 (2013) 278–284.
[38] A.V. Virkar, Y. Zhou, Mechanism of catalyst degradation in proton exchange membrane fuel cells, *J. Electrochem. Soc.* 154 (2007) B540.
[39] W. Bi, Q.H. Sun, Y.L. Deng, T.F. Fuller, The effect of humidity and oxygen partial pressure on degradation of Pt/C catalyst in PEM fuel cell, *Electrochim. Acta* 54 (6) (2009) 1826–1833.
[40] C. Lim, L. Ghassemzadeh, F.V. Hove, M. Lauritzen, J. Kolodziej, G.G. Wang, S. Holdcroft, E. Kjeang, Membrane degradation during combined chemical and mechanical accelerated stress testing of polymer electrolyte fuel cells, *J. Power Sources* 257 (2014) 102–110.
[41] P.C. Pei, H.C. Xu, X. Zeng, H.S. Zha, M.C. Song, Use of galvanostatic charge method as a membrane electrode assembly diagnostic tool in a fuel cell stack, *J. Power Sources* 245 (2014) 175–182.
[42] S. Kundu, M. Fowler, L.C. Simon, R. Abouatallah, Reversible and irreversible degradation in fuel cells during open circuit voltage durability testing, *J. Power Sources* 182 (1) (2008) 254–258.
[43] L. Ghassemzadeh, T.J. Peckham, T. Weissbach, X.Y. Luo, S. Holdcroft, Selective formation of hydrogen and hydroxyl radicals by electron beam irradiation and their reactivity with perfluorosulfonated acid ionomer, *J. Am. Chem. Soc.* 135 (42) (2013) 15923–15932.
[44] L. Ghassemzadeh, S. Holdcroft, Quantifying the structural changes of perfluorosulfonated acid ionomer upon reaction with hydroxyl radicals, *J. Am. Chem. Soc.* 135 (22) (2013) 8181–8184.